Published by
NIGERIAN SOCIETY OF PHYSICAL SCIENCES
Available online @ https://journal.nsps.org.ng/index.php/jnsps

J. Nig. Soc. Phys. Sci. 5 (2023) 1103

Journal of the Nigerian Society of Physical Sciences

Thermal distribution of magneto-tangent hyperbolic flowing fluid over a porous moving sheet: A Lie group analysis

A. B. Disu[a], S. O. Salawu[b,*]

[a]*Department of Mathematics, National Open University, Abuja, Nigeria*
[b]*Department of Mathematics, Bowen University, Iwo, Nigeria*

Abstract

An investigation of magneto-hyperbolic tangent fluid motion through a porous sheet which stretches vertically upward with temperature-reliant thermal conductivity is scrutinized in this study. The current model characterizes thermal radiation and the impact of internal heat source in the heat equation plus velocity and thermal slipperation at the wall. The translation of the transport equations is carried out via the scaling Lie group technique and the resultant equations are numerically tackled via shooting scheme jointly with Fehlberg integration Runge-Kutta scheme. The results are publicized through various graphs to showcase the reactions of the fluid terms on the thermal and velocity fields. From the investigations, it is found that rising values of the material Weissenberg number, slip and suction terms damped the hydrodynamic boundary film whereas the heat field is prompted directly with thermal conductivity.

DOI:10.46481/jnsps.2023.1103

Keywords: Thermal conductivity, Magneto-Tangent hyperbolic liquid, Porous sheet, Scaling Lie group, Thermal radiation

Article History :
Received: 03 October 2022
Received in revised form: 03 November 2022
Accepted for publication: 11 December 2022
Published: 24 February 2023

Communicated by: T. Latunde

1. Introduction

Magnetohydrodynamic is the interaction of an electromagnetic field with conducting fluids. Rheostat flow kinematics is a realistic application of magnetohydrodynamic where a magnetic field is used in conventional fluids since the heat exchange rate is unavailable for some sheet materials. Other uses include; thermal insulation, power storage, and so on. In the light of this, Abbas et al. [1] investigated a lateral stretching sheet of MHD power-law fluid with differing thermal conductivity. The authors reported a shrinking boundary layer structure with growth in the magnetic field term at all phase of fluid categories considered in the report. More so, Salawu et al. [2] analyzed magnetohydrodynamic viscous liquid flow across a nonlinear stretchy plate where the model ordinary derivative equations of the system was solved using the collocation-approximation. Sarkar and Makinde [3] explored the viscous fluids heat transport and magnetohydrodynamic flow across an exponentially stretching layer accounting for viscous dissipation and radiation effect. Nadeem et al. [4] explored the Magnetohydrodynamic rheological fluid flow on an angular boundary layer flow. The analysis showed that a boost in the magnetic field strength, the regular and tangential velocity profiles diminish while the skin friction coefficient increase.

Meanwhile, the studies conducted on the flow along a stretch-

*Corresponding author tel. no: +234 8032056439
Email address: kunlesalawu2@gmail.com (S. O. Salawu)

ing sheet has become a great deal of interest among researchers in respect of significant contributions in manufacturing and engineering activities. Sakiadis [5] analyzed the continuously moving flat surface on a laminar boundary layer and obtained a computational solution for the boundary layer equations. Crane [6] extended this by reporting on the time-independent linearly stretchy flow and specified the solutions in a closed form. Such a study was also extended by Wang [7] by incorporating partial slip effect, whereas Tshivhi et al. [8] investigated such a concept over a flat stretchable sheet when the flow is initiated spontaneously from rest. Okedoye et al. [9] analyzed slip fluid motion confined in a permeable stretchable material while the impact of partial slip due to vertical stretching sheet on stagnation-point flow with thermal transport was assessed by Zaimi and Ishak [10]. Salawu et al. [11] examined the cross-diffusion impact on magnetohydrodynamic fluid flow through a stretched sheet with velocity slip. A case of MHD dissipative fluid flow occasioned by a non-linearly stretched material with heat-mass transfer was numerically evaluated by Upreti et al. [12]. It was pointed out from the analysis that the thermal field is enlarged by the enhancement of the magnetic field. Such an investigation was also extended to the transport of Casson liquid configuration in a three-dimensional sheet with pores and Joule heating effect by Sreenivasulu et al. [13] while Fatunmbi and Okoya [14] inspected hydromagnetic micropolar fluid thermal transport characteristics over a stretching material featuring the prescribed thermal flux and plate temperature heating conditions.

The studies of non-Newtonian fluids have inspired scientists and engineers in recent times owing to its many uses in science and technology including food processing, drug and pharmaceutical productions, chemical engineering works and many more, Salawu et al. [15-16]. Examples of non-Newtonian fluids include gels, paints, blood, printers ink, lubricants with polymer ingredients, cosmetics and toiletries. Among various non-Newtonian fluid theories, there exists the tangent hyperbolic fluid model commonly utilized in numerous laboratory and chemical engineering processes. This fluid model displays a shear thinning attributes such that there exists a decline in the viscosity as the shear rate rises, Hassan et al. [17]. This unique feature of tangent hyperbolic fluid makes it a sought after in bio-engineering operations, for instance, the thinning attributes of blood flow in the body serves as a prevention to the obstruction of arteries and veins such that coagulation effect is minimized, Alsharif et al. [18]. In view of such striking characteristics, various researchers have applied this fluid model to analyze various flow problems under different configurations. Mamatha et al. [19] examined the motion of hydrodynamic tangent hyperbolic liquid mixed with dust particles in a porous stretching plate with convective heating. A numerical evaluation of such a phenomenon towards a stagnation-point in the occurrence of radiative heat, nonlinear convection, haphazard motion and thermo-migration of nanoparticles was scrutinized by Khan et al. [20]. Meanwhile, the distribution of such a liquid with nanomaterials mixture in a nonlinear stretchable material was scrutinized by Mahanthesh and Mackolil [21] for a stagnation fluid. These researchers reported a rise in the viscous drag due to enhancement in the power-law index and magnetic field terms. Oyelakin and Sibanda [22] inspected the influence of exponentially based viscosity on the motion of hyperbolic tangent fluid. The report showed that a decrease in the viscosity triggered a spike in the velocity while lowering the heat and species intensity.

Sophus and Ackerman [23] found point metamorphosis that mapped a given differential equation and introduced the Lie group analysis classical approach. This approach brings together nearly every known technique of exact integration for all the associated ordinary and partial differential equations. Many researchers employed this technique to determine the similarities among given differential equations. Using this technique, the number of variables that control the partial differential systems can be effectively reduced, Salawu and Dada [24]. The dilution of values transforms the partial differential system into ordinary systems. Using Lie group analysis approach, convective dynamics problems have been studied on different flow configurations in various science and engineering branches, Zakir and Zaman [25]. Similarly, Ullah and Zaman [26] engaged this approach while studying the transport and thermal effects of a tangent hyperbolic flowing liquid through a stretched plate with Navier slip effect. Further, Ullah et al. [27] engaged this approach to extend the work of [26] by incorporating suction/injection coupled with heat generation. The authors examined the partial differential equations representing a natural convective unstable flow movement using the Lie symmetry transformation approach. The classical Lie group transformation is applied twice sequentially in this study to change the transport model into a set of ordinary derivative equation.

The above studies however ignored the impact of variable heat conduction in the temperature field. Thermal conductivity describes the characteristic quantity of fluids that allows them to conduct heat. For accurate prediction of thermal propagation processes, the influence of temperature-based thermal conductivity has to be considered. Shahzad et al. [28] investigated such an effect on a viscous fluid in the existence of a stretching layer by utilizing the shooting process and the perturbation procedure in analyzing the numerical solution. Similarly, Alsherif et al. [29] took into account the case of a stretching cylinder, considered a viscous fluid flow alongside variable thermal conductivity. The investigation depicted that growing the curvature of the cylinder causes the fluid temperature to rise rapidly. An examination of temperature based thermal conductivity coupled with thermal radiation impact of a viscous fluid in a porous stretching material was evaluated by Hayat et al. [30]. Ullah et al. [31] reported on power-law convective MHD liqud flow across a linearly stretchy plate alongside thermal conductivity influence. Recently, such a concept has been widely investigated by various researchers, Aziz and Shams [32] on diverse flow configurations and conditions.

In view of the discussion above and the consequential applications of essential fluids parameters in manufacturing and engineering works, the present work aim to determine the motion and thermal transport of hydromagnetic tangent hyperbolic liquid over a permeable vertical stretchy surface using Lie group analysis approach. In particular, this study extends that of [26,

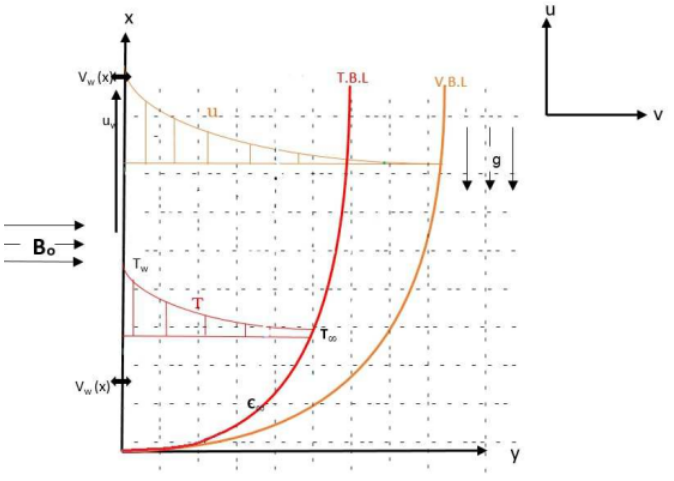

Figure 1. Configuration of the flow model

31] by considering porous media with the inclusion of variable heat conductivity, thermal radiation and a buoyancy effect which were ignored by previous authors. A unique similarity transformation approach is developed using the Lie group analysis which is adopted for transforming the nonlinear partial derivative transport model into a more simplified ordinary derivative form. The resultant set of outlining equations is numerically tackled using the shooting algorithm in conjunction with Fehlberg integration Runge-Kutta method. The physical characteristics of dimensionless terms obtained are clarified using graphs with appropriate discussion.

2. Problem Formulation Analysis

The underlisted assumptions have been identified as crucial for the formulation of the governing equations for the current investigation. Is is assumed that the fluid movement is time-independent, incompressible tangent hyperbolic fluid. The fluid movement is designed in a two-dimensional porous plate which stretches upwardly in a vertical route as displayed in Figure 1. The flow is routed in x axis while y axis runs perpendicular to x axis. A restriction is placed on the flow in the region $y > 0$. There is slippery in the momentum and energy boundary layers. There is a surface mass flux on the sheet having a velocity of $v_w(x)$ as expressed in Eq. (7). With the imposition of an external magnetic field normal to x direction but ignoring that of the induced magnetic filed influence and electric field as well. Likewise, it is supposed that the radiative heat flux is negligible towards the x axis whereas it is applicable along y direction. Furthermore, the assumption of varying thermal conductivity is held valid with the inclusion of heat source. Other fluid attributes are are constant apart from the non-uniformity of the density in the momentum body force and the thermal conductivity. Boussinesq approximation coupled with boundary layer approximation are applied in this study for the derivation of the main equations. For this study, the tangent hyperbolic fluid tensor is described as [26,31]

$$\overline{\tau} = [\mu_\infty + (\mu_0 + \mu_\infty)\tanh(\Gamma\overline{\gamma})^m]\overline{\gamma}, \tag{1}$$

In Eq. (1), $\overline{\tau}$ describes the tensor stress while μ_∞ depicts viscous shear rate at infinity whereas μ_0 signifies the zero viscous shear rate and Γ describes the material constant of time-dependent whereas m connotes the power-law exponent while $\overline{\gamma}$ is expressed as:

$$\overline{\gamma} = \left(\frac{1}{2}\Sigma_i\Sigma_j\overline{\gamma}_{ij}\overline{\gamma}_{ji}\right)^{\frac{1}{2}} = \left(\frac{1}{2}\Pi\right)^{\frac{1}{2}}. \tag{2}$$

In Eq. (2), $\Pi = \frac{1}{2}tr((\nabla V)^T + \nabla V)^2$. The case $\mu_\infty = 0$ is accounted for owing to low influence of viscosity at infinity. Also taking into account the tangent hyperbolic fluid detailing shear thinning characteristics, with the assumption that $\Gamma\overline{\gamma} < 1$, Eq. (1) then reduces to:

$$\overline{\tau} = \mu_o[\Gamma\overline{\gamma}^m]\overline{\gamma} = \mu_o[(1 + \Gamma\overline{\gamma} - 1)^m]\overline{\gamma}$$
$$\approx \mu_o[(1 + m(\Gamma\overline{\gamma} - 1))]\overline{\gamma} \tag{3}$$

2.1. The Governing Equations

Combining the above-mentioned assumptions for the development of the transport model, Eqs. (4-6) describes the transport equations for the present investigation (see [20,26,31]).

$$\frac{\partial u}{\partial x} + \frac{\partial v}{\partial y} = 0, \tag{4}$$

$$u\frac{\partial u}{\partial x} + v\frac{\partial u}{\partial y} = (1-m)\,\nu\frac{\partial^2 u}{\partial y^2} + \sqrt{2}\nu m\Gamma\left(\frac{\partial u}{\partial y}\right)\frac{\partial^2 u}{\partial y^2} - \frac{\sigma B^2}{\rho}u + g\beta_T(T - T_\infty) - \frac{\nu}{k_p}u, \tag{5}$$

$$u\frac{\partial T}{\partial x} + v\frac{\partial T}{\partial y} = \frac{1}{\rho C_p}\frac{\partial}{\partial y}\left(k(T)\frac{\partial T}{\partial y}\right) - \frac{1}{\rho C_p}\frac{\partial q_r}{\partial y} + \frac{Q_o}{\rho C_p}(T - T_\infty) + \frac{\nu}{C_p k_p}u^2 + \frac{\sigma B^2}{\rho C_p}u^2, \tag{6}$$

The respective flow boundary constraints are stated below

$$u = cx + \beta\frac{\partial u}{\partial y},\ v = v_w(x),\ T = T_w + G\frac{\partial T}{\partial y}\ at\ y = 0, \tag{7}$$

$$u \longrightarrow 0, T \longrightarrow T_\infty\ as\ y \longrightarrow \infty. \tag{8}$$

The thermal flux radiation q_r in Eq. (6) is indicated in Eq. (9) as (see Sumalatha and Bandari [33])

$$q_r = -\left(\frac{4\sigma^*}{3k^*}\right)\frac{\partial T^4}{\partial y} \tag{9}$$

From the above Eqs.(4-9), u and v describe flow rtae modules in respect to x and y axes. The symbols k_p, β and σ represent porous medium permeability, velocity slip factor and electrical conductivity whereas the density, volumetric thermal expansion coefficient, magnetic flux density and the thermal slip factor are sequentially denoted by ρ, β_T, B and G. Also, T signals the fluid temperature, g denotes gravitational acceleration, ν is the kinematic viscosity, v_w describes surface mass flux, c defines

stretching rate and Q_o describes coefficient of heat source/sink, σ^* connotes Stefan-Boltzmann constant while the coefficient absorption mean is taken as k^*. By the application of the Rosseland approximation and assuming that the heat variation is low in the flow field, so that Taylor's series can utilized to expand T^4 to get

$$T^4 \approx 4T_\infty^3 - 3T_\infty^4,$$

The temperature-based thermal conductivity is also specified as (see Animasaun [34]):

$$k(T) = k_\infty[1 + \zeta(T - T_\infty)], \tag{10}$$

in which k_∞ denotes the upstream heat conduction, ζ typifies the thermal conductivity parameter. To transmute the outlining flow equations into dimensionless system, the underlisted quantities adopted:

$$\frac{\overline{x}}{x} = \left(\frac{a}{\nu}\right)^{\frac{1}{2}},\ \frac{\overline{y}}{y} = \left(\frac{a}{\nu}\right)^{\frac{1}{2}},\ \frac{\overline{u}}{u} = \frac{1}{(a\nu)^{\frac{1}{2}}},\ \frac{\overline{v}}{v} = \frac{1}{(a\nu)^{\frac{1}{2}}},$$
$$T = (T_w - T_\infty)\theta + T_\infty. \tag{11}$$

Dropping the bar and substituting $u = \frac{\partial\psi}{\partial y}$ and $v = -\frac{\partial\psi}{\partial x}$ into Eqs. (5-6) taking cognizance Eqs (9) and (10), the underlisted are obtained

$$\left(\frac{\partial\psi}{\partial y}\frac{\partial^2\psi}{\partial x\partial y} - \frac{\partial\psi}{\partial x}\frac{\partial^2\psi}{\partial y^2}\right) = (1-m)\frac{\partial^3\psi}{\partial y^3} + \sqrt{2}ma\Gamma\left(\frac{\partial^2\psi}{\partial y^2}\right)\frac{\partial^3\psi}{\partial y^3} - \left(\frac{\sigma B^2}{a\rho} + \frac{\nu}{ak_p}\right)\frac{\partial\psi}{\partial y} + \frac{gB_T(T_w - T_\infty)}{a^{\frac{3}{2}}\nu^{\frac{1}{2}}}\theta, \tag{12}$$

$$\left(\frac{\partial\psi}{\partial y}\frac{\partial\theta}{\partial x} - \frac{\partial\psi}{\partial x}\frac{\partial\theta}{\partial y}\right) = \left(\frac{k_\infty}{\mu c_p}(1+\zeta\theta) + \frac{16\sigma^*}{3\mu c_p k^*}T_\infty^3\right)\frac{\partial^2\theta}{\partial y^2} + \frac{k_\infty}{\mu c_p}\zeta\left(\frac{\partial\theta}{\partial y}\right)^2 + \frac{Q_o}{a\rho C_p}\theta + \frac{u_w^2\sigma B^2}{a\rho C_p(T_w - T_\infty)}\left(\frac{\partial\psi}{\partial y}\right)^2 + \frac{u_w^2\nu}{ak_p\rho C_p(T_w - T_\infty)}\left(\frac{\partial\psi}{\partial y}\right)^2, \tag{13}$$

Also, the boundary conditions (7-8) transform to:

$$\frac{\partial\psi}{\partial y} = \frac{c}{a}x + \beta\sqrt{\frac{a}{\nu}}\frac{\partial^2\psi}{\partial y^2},\ \frac{\partial^2\psi}{\partial x^2} = \frac{v_w}{\sqrt{a\nu}},\ \theta = 1 + G\sqrt{\frac{a}{\nu}}\frac{\partial\theta}{\partial y}\ at\quad y = 0,$$
$$\frac{\partial\psi}{\partial y} \to 0,\ \theta \to 0\ as\ y \to \infty. \tag{14}$$

3. Lie Group Scaling Transformations

The Lie scaling technique depends on theory formulated to find all symmetry transformations that keep the system of equations unchanged. It helps in reducing the number of independent variables and in consequence transforms the PDEs to an ODEs. Using this method to generate similarity variables involves finding the invariant solution which does not alter the structure of the given equation under study. In this section, the simplified format of the Lie group transformation approach is employed to derive the new similarity transformations for the transport equations. As such, the outlining flow equations can be changed to ordinary derivative equations. Following [27,31,35] the transformation variables are defined

$$\Upsilon : x^* = xe^{\varepsilon\gamma_1},\ y^* = ye^{\varepsilon\gamma_2},\ \psi^* = \psi e^{\varepsilon\gamma_3},\ \theta^* = \theta e^{\varepsilon\gamma_4},\ \Gamma^* = \Gamma e^{\varepsilon\gamma_5} \tag{15}$$

In Eq. (15), ε depicts the parameter of the group whereas the transformation variables are represented by $\gamma_1, \gamma_2, \gamma_3, \gamma_4, \gamma_5$. Also, Eq. (15) is called point transformation for the set of coordinates system $(x, y, \psi, \theta, \Gamma)$ transforms into $(x^*, y^*, \psi^*, \theta^*, \Gamma^*)$. The substitution of the transformation Eq. (15) into Eq. (12) and (13) results to the form:

$$\begin{aligned} &e^{\varepsilon(\gamma_1+2\gamma_2-2\gamma_3)}\left(\frac{\partial\psi^*}{\partial y^*}\frac{\partial^2\psi^*}{\partial x^*\partial y^*} - \frac{\partial\psi^*}{\partial x^*}\frac{\partial^2\psi^*}{\partial y^{*2}}\right) \\ &= e^{\varepsilon(3\gamma_2-\gamma_3)}(1-m)\frac{\partial^3\psi^*}{\partial y^{*3}} \\ &+ e^{\varepsilon(5\gamma_2-2\gamma_3-\gamma_5)}\left(\sqrt{2}m\Gamma\left(\frac{\partial^2\psi^*}{\partial y^{*2}}\right)\frac{\partial^3\psi^*}{\partial y^{*3}}\right) \\ &- e^{\varepsilon(\gamma_2-\gamma_3)}\left(\frac{\sigma B^2}{a\rho} + \frac{\nu}{ak_p}\right)\frac{\partial\psi^*}{\partial y^*} + \frac{gB_T(T_w - T_\infty)}{a^{\frac{3}{2}}\nu^{\frac{1}{2}}}\theta^* e^{-\varepsilon\gamma_4}, \end{aligned} \tag{16}$$

$$\begin{aligned} &e^{\varepsilon(\gamma_1+\gamma_2-\gamma_3-\gamma_4)}\left(\frac{\partial\psi^*}{\partial y^*}\frac{\partial\theta^*}{\partial x^*} - \frac{\partial\psi^*}{\partial x^*}\frac{\partial\theta^*}{\partial y^*}\right) \\ &= e^{\varepsilon(2\gamma_2-\gamma_4)}\left(\frac{k_\infty}{\mu c_p}(1+\zeta\theta^*) + \frac{16\sigma^*}{3\mu c_p k^*}T_\infty^3\right)\frac{\partial^2\theta^*}{\partial y^2} + \\ &e^{\varepsilon(2\gamma_2-2\gamma_4)}\frac{k_\infty}{\mu c_p}\zeta\left(\frac{\partial\theta^*}{\partial y^*}\right)^2 + \frac{Q_o}{a\rho C_p}\theta^* e^{-\varepsilon\gamma_4} \\ &+ e^{\varepsilon(\gamma_2-\gamma_3)}\left(\frac{u_w^2\sigma B^2}{a\rho C_p(T_w - T_\infty)} + \frac{u_w^2\nu}{ak_p\rho C_p(T_w - T_\infty)}\right)\left(\frac{\partial\psi^*}{\partial y^*}\right)^2, \end{aligned} \tag{17}$$

Similarly, the boundary conditions transform to:

$$\begin{aligned} &e^{\varepsilon(\gamma_2-\gamma_3)}\frac{\partial\psi^*}{\partial y^*} = \frac{c}{a}e^{-\varepsilon\gamma_1}x^* + \beta\sqrt{\frac{a}{\nu}}\frac{\partial^2\psi^*}{\partial y^{*2}}e^{\varepsilon(2\gamma_2-\gamma_3)}, \\ &\frac{\partial^2\psi^*}{\partial x^{*}2}e^{\varepsilon(\gamma_2-\gamma_3)} = \frac{v_w}{\sqrt{a\nu}}, \\ &e^{-\varepsilon\gamma_4}\theta^* = 1 + G\sqrt{\frac{a}{\nu}}\frac{\partial\theta^*}{\partial y^*}e^{\varepsilon(\gamma_2-\gamma_4)} \quad at \quad e^{-\varepsilon\gamma_1}y^* = 0, \\ &e^{\varepsilon(\gamma_2-\gamma_3)}\frac{\partial\psi^*}{\partial y^*} \to 0,\ e^{-\varepsilon\gamma_4}\theta^* \to 0\ as\ y^* \to \infty. \end{aligned} \tag{18}$$

The preceding system of equations is invariant under the group transformation if the underlisted relationship exist among the exponents:

$$\gamma_1 + 2\gamma_2 - 2\gamma_3 = 3\gamma_2 - \gamma_3 = 5\gamma_2 - 2\gamma_3 - \gamma_5 = \gamma_2 - \gamma_3 = -\gamma_4 \tag{19}$$

$$\gamma_1 + \gamma_2 - \gamma_3 - \gamma_4 = 2\gamma_2 - \gamma_4 = 2\gamma_2 - 2\gamma_4 = -\gamma_4 \tag{20}$$

solving Eq. (19) and (20) to obtain the following relations:

$$\gamma_1 = \gamma_3, \gamma_2 = 0, \gamma_4 = \gamma_1, \gamma_5 = -\gamma_1 \tag{21}$$

Eq. (21) can then be introduced into Eq. (15) to obtain the criterion for the transformation as:

$$\Upsilon : x^* = xe^{\varepsilon\gamma_1}, y^* = y, \psi^* = \psi e^{\varepsilon\gamma_1}, \theta^* = \theta, \Gamma^* = \Gamma e^{-\varepsilon\gamma_1} \tag{22}$$

Applying Taylor's series to expand Eq. (22) in the power of ε to the first order to obtain:

$$x^* - x = x\varepsilon\gamma_1,\ y^* - y = 0,\ \psi^* - \psi\varepsilon\gamma_1,$$
$$\theta^* - \theta = 0,\ \Gamma^* - \Gamma = -x\varepsilon\gamma_1, \tag{23}$$

Taking Eq. (23), the following characteristic equation were obtained:

$$\frac{dx}{x\gamma_1} = \frac{dy}{0} = \frac{d\psi}{x\gamma_1} = \frac{d\theta}{0} = \frac{d\Gamma}{-x\gamma_1}, \tag{24}$$

the following similarity transformations are derived by solving Eq. (24) (see Ulla and Zaman, 2017):

$$\eta = y,\ \psi = xf(\eta),\ \theta = \theta(\eta),\ \Gamma = x^{-1}\Gamma_o \tag{25}$$

The non-dimensional ODEs obtained with corresponding boundary condition via the similarity transformations (25) into Eqs. (16-18) are as follows:

$$(1-m)f''' + mW_e f'''(f'') + ff'' - (M^2 + Da)f'$$
$$-(f')^2 + Gr\theta' = 0 \tag{26}$$

$$(1 + \zeta\theta + Nr)\theta'' + \zeta\theta'^2 + Pr(Q\theta + f\theta')$$
$$+ PrEcM^2 f'^2 + PrEcDaf'^2 = 0 \tag{27}$$

$$f'(0) = \lambda + \alpha f''(0),\ f(0) = S,\ \theta(0) = 1 + \theta'(0), \tag{28}$$

$$f' \to 0,\ \theta \to 0 \quad as \quad \eta \to \infty. \tag{29}$$

In Eqs. (26-29), $W_e = \sqrt{2}a\Gamma$ symbolizes the Weissenberg number, $Nr = \frac{16\sigma^*}{3k^*k}T_\infty^3$ defines radiation parameter, $M^2 = \frac{\sigma B^2}{a\rho}$ denotes Hartmann number, $Q = \frac{Q_0}{a\rho c_p}$ typifies the heat source/sink factor and $b = \sqrt{\frac{a}{\nu}}G$ is the thermal slip parameters whereas $\alpha = \sqrt{\frac{a}{\nu}}\beta$ represents the velocity slip, $Da = \frac{\nu}{ak_p}$ characterizes the Darcy number and ζ implies thermal conductivity parameter. The primes signifies differential with respect to η, $\lambda = \frac{c}{a}$ is the stretching parameter, $Ec = \frac{u_w^2}{C_p(T_w - T_\infty)}$ is Eckert number, $Gr = \frac{gB_T(T_w - T_\infty)}{a^{\frac{3}{2}}\nu^{\frac{1}{2}}x}$ symbolizes the Grashof number, $S = \frac{v_w}{\sqrt{a\nu}}$ is the mass suction and $Pr = \frac{\mu c_p}{k_\infty}$ represents the Prandtl number. The incorporated engineering quantities in the current investigation include the wall friction Cf_x and the thermal gradient Nu_x which are orderly specified in Eq. (30) as:

$$\rho(ax)^2 Cf_x = \tau_w,\ Nu_x = \frac{xq_w}{k(T_w - T_\infty)} \tag{30}$$

Table 1. Skin friction coefficient as compared with previous studies when $W_e = m = 0$

M	Akbar [36]	Fathizadeh et al. [37]	Present values
0	1.00000	1.00000	1.00000
1	−1.41421	−1.41421	−1.41421
5	−2.44948	−2.44948	−2.44949
10	−3.31662	−3.31662	−3.31663
50	−7.14142	−7.14142	−7.14143
100	10.0499	10.0499	10.0499
500	−22.38300	−22.38300	−22.38300

where

$$\tau_w = (1-m)\frac{\partial u}{\partial y} + \frac{m\Gamma}{\sqrt{2}}\left(\frac{\partial u}{\partial y}\right)^2\Bigg|_{y=0},$$
$$q_w = -k_\infty\left(1 + \frac{16\sigma^*}{3k^*k_\infty}T_\infty^3\right)\frac{\partial T}{\partial y}\Bigg|_{y=0} \tag{31}$$

The dimensionless form of Eq. (30) are specified in Eq. (31) as:

$$Re^{\frac{1}{2}}C_f = [(1-m)f''(0) + \frac{m}{2}W_e(f''(0))^2],$$
$$Re^{-\frac{1}{2}}Nu_x = -(1 + Nr)\,\theta'(0), \tag{32}$$

where $Re_x = \frac{ax^2}{\nu}$ signifies the local Reynolds number.

4. Numerical Solution

Eqs. (26-27) comprises of a set nonlinear coupled differential equations with it's associated wall conditions. Owing to the non-linearity nature of the governing equations, Eqs (26-27) subject to (28-29) are tackled numerically using shooting techniques alongside Runge-Kutta Fehlberg scheme by utilizing a computer algebra symbolic code of Maple software. This algorithm relies on the adopted method. Except otherwise, the subsequent default values as been adopted for the study based on related previous analysis as $n = 0.4$, $We = 0.3$, $\epsilon = 0.2$, $Nr = 0.3$, $M = 0.2$, $Da = 0.3$, $Pr = 3.0$, $Q = 0.3$, $Gr = 2.0$, $Ec = 0.01$, $\lambda = 0.7$, $S = 0.3$, $\alpha = 0.2$, $b = 0.5$. The numerical code's accuracy is validated by assessing the computational outcomes of the wall drag coefficient C_{fx} offered in this study as compared with previously published works of Akbar [36] and Fathizadeh et al. [37] in respect to variations in the Hartmann number (M). As recorded in Table 1, the comparison showed a perfect harmony with the existing data in the literature under limiting circumstances and thus confirming the accuracy of our numerical code. Table 2 depicts the influences of some entrenched parameters on the wall friction and heat gradient. As seen, an enhance or decline in the engineering quantities are observed due to the boundary layer viscosity. When the boundary film viscidness is stimulated the wall friction and Nusselt effect are raised, but when thinner boundary film viscidness noticed the diffuse more to the ambient leading to a decrease in the wall effects.

Table 2. Numerical values for the skin friction (Cf), heat gradient (Nu_x)

M	ϵ	λ	Da	We	Ec	Q	Cf	Nu_x
0.2	0.2	0.7	0.3	0.3	0.01	0.3	0.8722973797	-0.5937107035
0.5							0.7677915589	-0.56754883934
1.0							0.4376848220	-0.48222768379
	0.4						0.9077648755	-0.53183984435
	0.7						0.9077648765	-0.53183984435
		1.0					0.4765432364	-0.67408773863
		1.5					0.2732784056	-0.80313254770
			0.7				0.6779856282	-0.54475633672
			1.0				0.6779856282	-0.54475633672
				0.5			0.8498608064	-0.59162423311
				0.7			0.8300639857	-0.58974089749
					0.03		0.8735104313	-0.59064728168
					0.07		0.8735104313	-0.59064728168
						1.0	1.1540832041	0.0316335380
						2.0	1.8442011437	1.9856306670

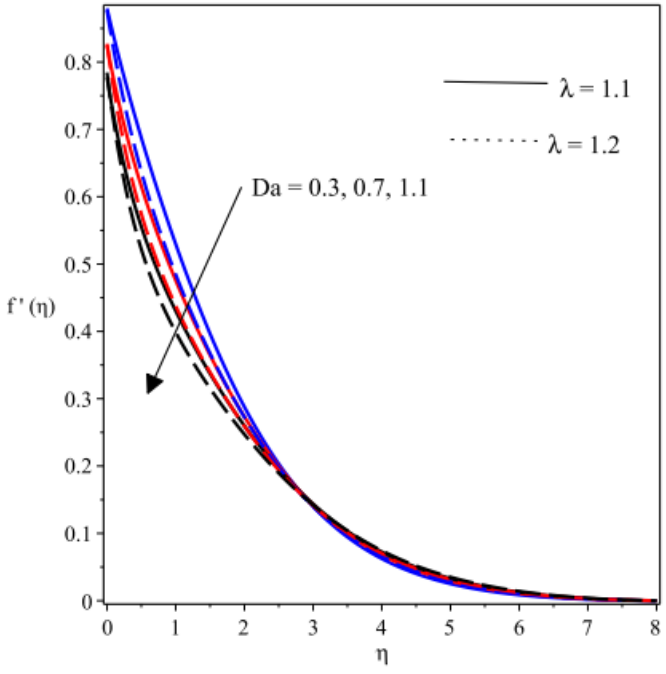

Figure 2. Plot of $Da\&\lambda$ on velocity $f'(\eta)$

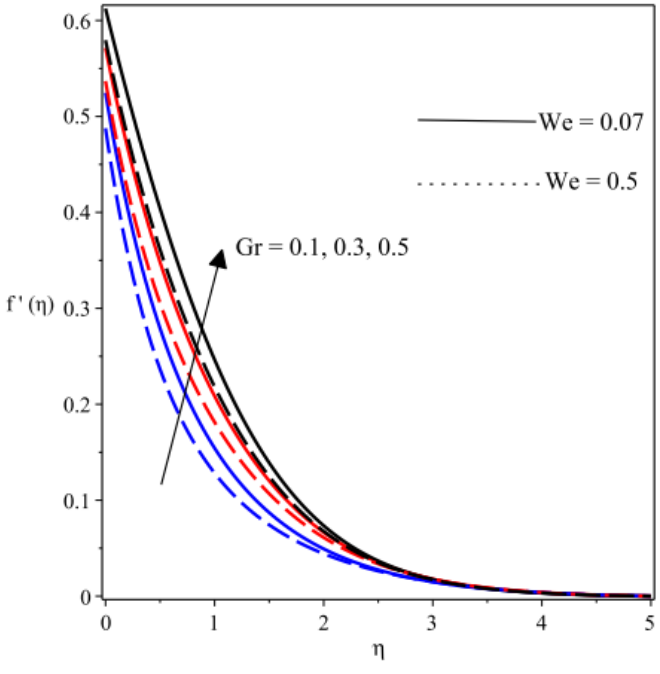

Figure 3. Behaviour $Gr\&We$ on velocity $f'(\eta)$

5. Discussion of Outcomes

This aspect displays and discusses the reactions of the dimensionless flow rate and energy profiles due to variations in the physical flow parameters. These physical parameters include the stretchy term (λ), Grashof (Gr), Prandtl (Pr), Weissenberg (We) and Darcy (Da) numbers, heat source term (Q), power-law exponent term (m), velocity slip term (α), radiation parameter (Nr), Hartmann number (M), mass suction parameter (S), thermal conductivity parameter (ζ), and temperature slip term (b).

Figures 2-6 describe the influences of various physical flow parameter on the velocity field. Fig. 2 illustrates the effects of (Da) Darcy term on the dimensionless velocity in the existence of stretching parameter (λ). Evidently, there is a decrease in the velocity as (Da) increases. The flow behaviour in respect to a spike in Darcy number (Da) stimulates an opposition to the flow distribution that leads to a shrink boundary layer and thereby decelerates the fluid motion. In a related sense, an enhancement in the magnitude of the stretching term (λ) lowers the momentum boundary layer structure and consequently decelerates the locomotion. The impacts of Grashof number (Gr) and Weissenberg term (We) on the dimensionless flow rate profile are presented in Fig. 3. It is evident from the graph displayed that the velocity drop significantly by a rise in (We) owing to an increase in the viscosity whereas there is an acceleration in the

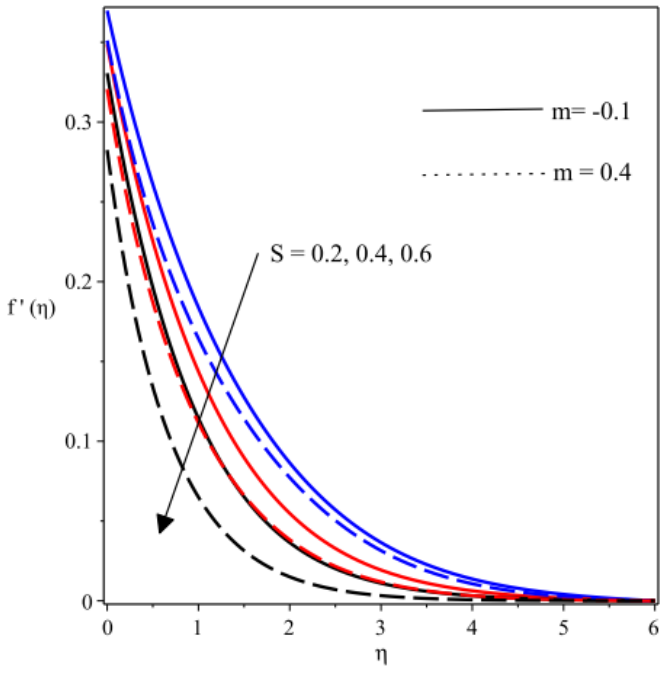

Figure 4. Effect of S &m on velocity $f'(\eta)$

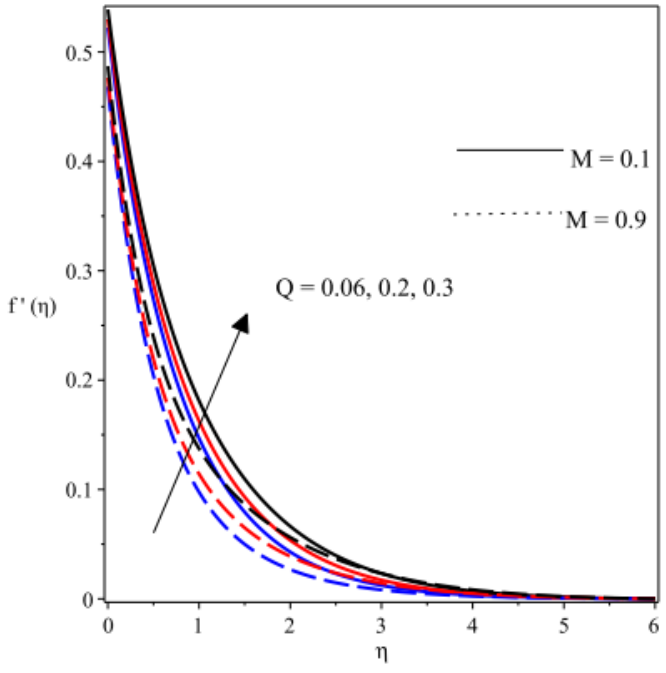

Figure 5. Reaction Q&M on velocity $f'(\eta)$

fluid motion as Grashof number increases due to enhancement in the buoyancy force. As (Gr) is raised, the buoyancy force dominates the viscous force and thus encourages the velocity distribution. Fig. 4 portrays the impact of mass suction term (S) coupled with that of the power-law exponent (m) on the velocity distribution. It is evident that enhancing the magnitude of the power-law exponent (m) raised the viscosity and as a result, there is a significant drop in fluid velocity. Also, this plot

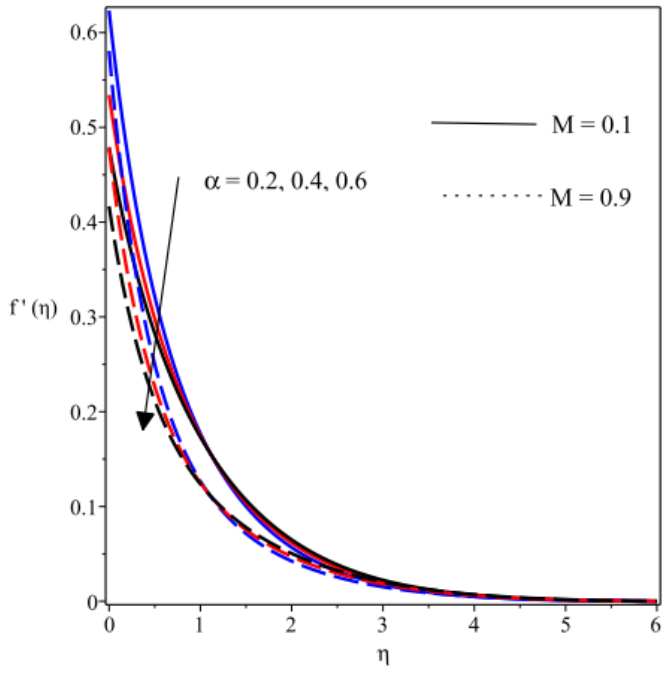

Figure 6. Effect of α&M on velocity $f'(\eta)$

shows raising the magnitude of S and (m), the hydrodynamic boundary structure thickness declines and the velocity decelerates. The evaluation of the heat generation (Q) term and the Hartmann number (M) is plotted in Fig. 5. Evidently, an electromagnetic force is produced from the magnetic field interaction with the tangent hyperbolic electrically conducting liquid that create a drag in the flow movement as noted in the plot. The electro-conducting fluid's interaction with the transverse magnetic field induces a retarding force on the liquid motion. Similarly, a hike in (Q) induces higher flow velocity rate owing to a decrease in the viscosity. Fig. 6 offers the behaviour of (α) on the liquid motion. In this plot, a declining trend is observed in the velocity field as the slip term (α) rises.

Figures 7-12 offer the variations of some physical terms on the thermal field. Firstly, the temperature profile showing the impact of (λ) in the occurrence of radiative heat (Nr) parameter is plotted in Fig 7. The graph elucidates that advancement in (λ) causes the temperature to fall whereas growing (Nr) enhances the thermal profile. An advancement in the radiative heat flux corresponding to a rise in Nr while the Rosseland mean absorption coefficient declines and as such, the thermal field is enhanced as found in this figure. The results of the Prandtl number (Pr) and power-law index (m) on the thermal distribution are depicted in Fig. 8. The graph demonstrates that a boost in the (Pr) number lowers the thermal field by shrinking the energy boundary viscosity structure whereas the thermal propagation improves as (m) rises. The Prandtl number connotes the diffusivity of the momentum ratio to the diffusivity of the heat, and also influence the relative momentum shear stress and thermal boundary layer. Thus, a boost in the Pr implies a reduction in the energy boundary film and consequently leads to a decline in the heat transfer. The reactions of thermal generation term

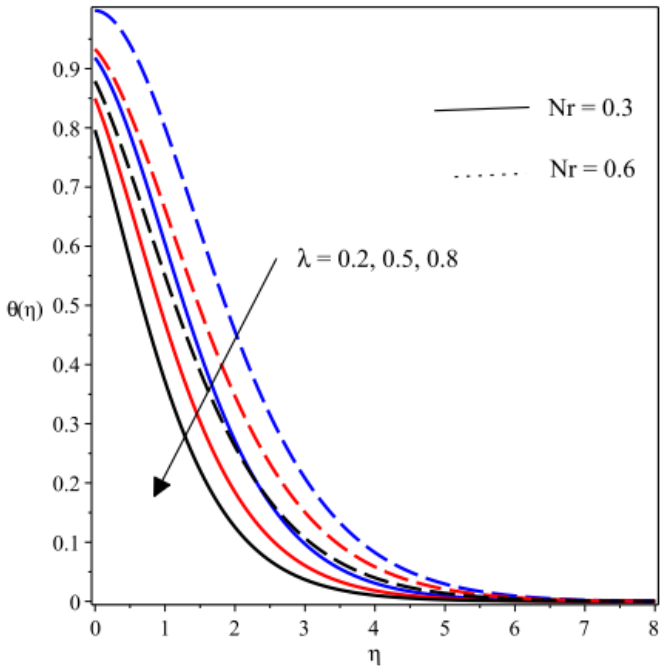

Figure 7. Influence of λ&Nr on temperature $\theta(\eta)$

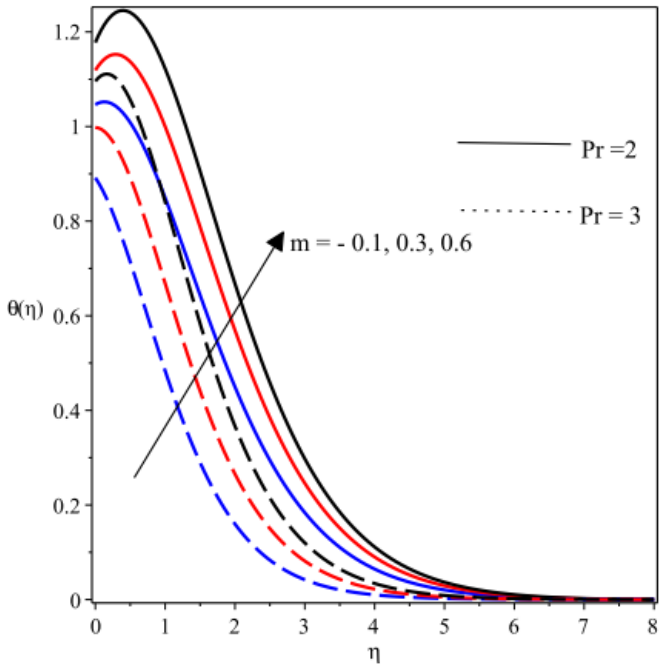

Figure 8. Reactions of m&Pr on temperature $\theta(\eta)$

(Q) and Hartmann term (M) on the energy filed are displayed in Fig. 9. The graph portrays the fluid temperature exhibiting identical growing patterns on (Q) and (M). Typically, both parameters cause a rising trend in the thermal boundary layer. An enhancement in (M) induces a higher electromagnetic force which inspires an obstruction to the liquid motion and thus increase frictional heating effect which boosts the surface temperature. Similarly, a hike in Q is an indication of extra energy being generated and thus, a rise in the temperature as found in this figure.

Fig. 10 elucidates the reactions of the thermal slip term (b) and Weissenberg term (We) on the fluid heat propagation. The temperature boundary structure shrinks and the temperature falls with growth in b whereas the converse occurs with enhancement in We as noticed in this figure. A rise in (b) draws away the fluid from the heated region thereby lowers the temperature whereas as We rises in magnitude a frictional heat is generated due to rising viscosity. The reactions of mass suction term (S) and power-law exponent (m) are plotted in Fig. 11. This plot reveals that with advancement in S, the temperature distribution subsides whereas as (m) increases, the temperature distribution shoots up. Likewise, the plot showing the variation in Darcy term (Da) and thermal conductivity term ζ in respect to temperature is sketched in Fig. 12. It is noticeable that an increment in the (Da) and ζ boost the temperature distribution due to extra heat generated by the resistance imposed on the fluid flow as Da increases. In Figure 13, the impact of Ecket number (Ec) on the heat propagation with variation in Hartmann number (M) is established. As seen, temperature distribution is raised due to an induce magnetic Joule heating that inspired the tangent hyperbolic fluid flow particles interaction. Also, the magnetic Joule heating effect is complemented

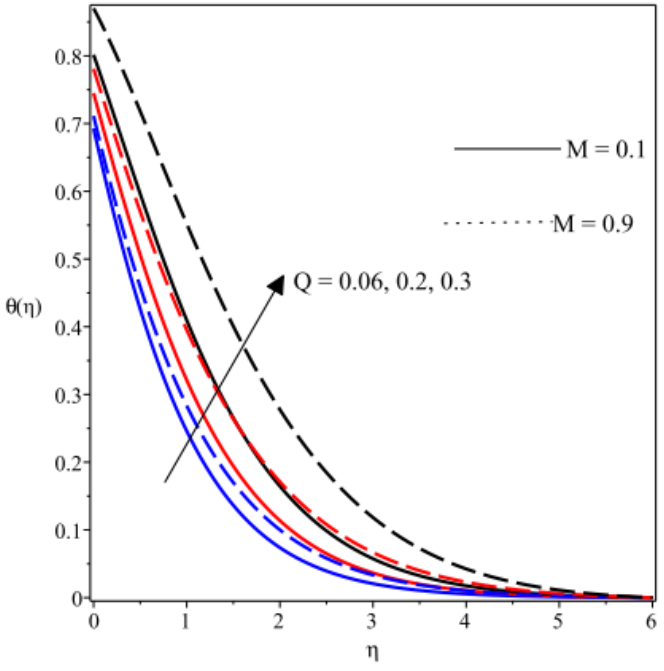

Figure 9. Impact of Q&M on temperature $\theta(\eta)$

by the porous Joule heating that creates fluid friction and resistant to free flow, thus, particles collision and random motion is encouraged to increase heat transfer. Therefore, rising heat distribution magnitude is observed all over the flow region.

6. Conclusion

A computation solution has been performed on the motion and thermal propagation of hydromagnetic tangent hyperbolic

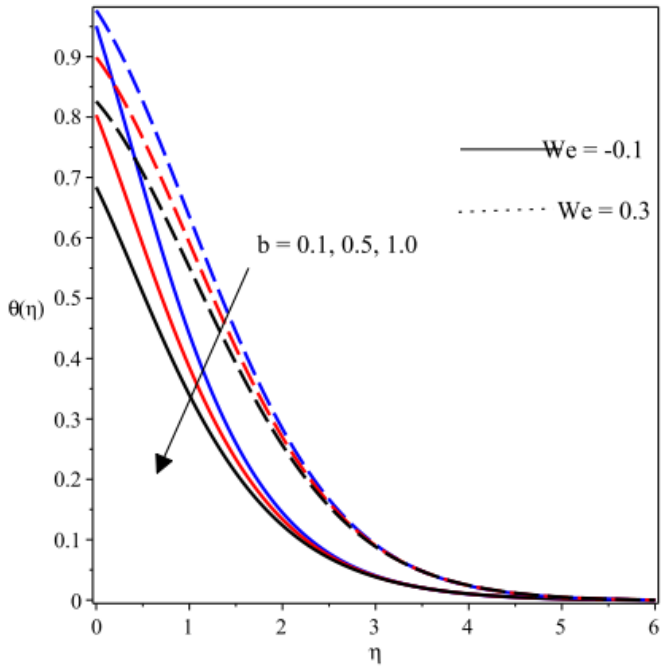

Figure 10. Impact of b&We on temperature $\theta(\eta)$

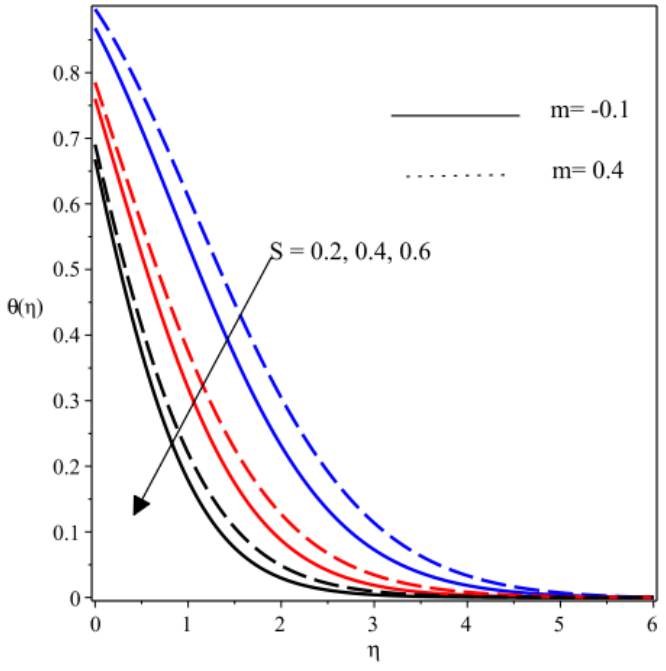

Figure 11. Effect of S &m on $\theta(\eta)$

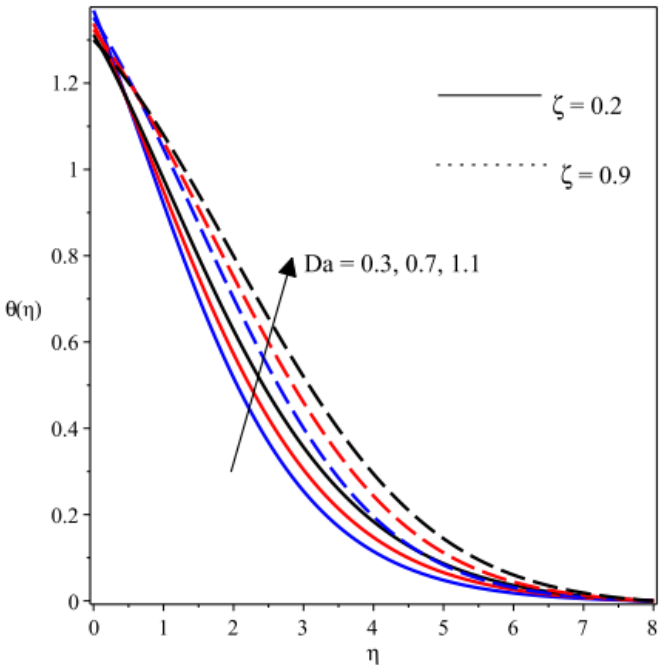

Figure 12. Influence of Da&ζ on temperature $\theta(\eta)$

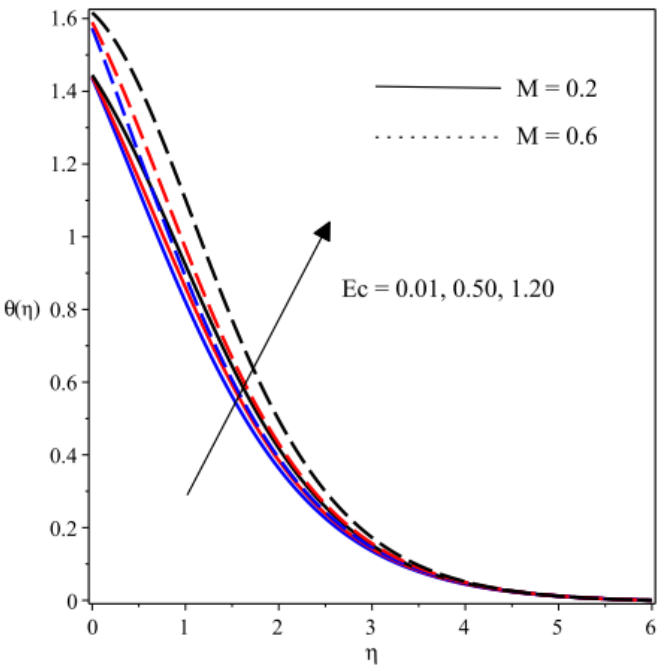

Figure 13. Effect of Ec&M on heat field $\theta(\eta)$

liquid passing a vertically stretched surface with varying thermal conductivity. The flow model is in steady 2-dimensional and incompressible stretchable plate enclosed in permeable media with the impact of radiative heat and internal thermal energy source. Lie group analysis generates the similarity transformation which transformed the coupled differential equations with boundary conditions from partial to ordinary derivative equations, The solution to the equations are the offered computationally via shooting approach alongside Fehlberg Runge-Kutta method. The solutions are given graphically and deliberated while comparison with published studies show good agreement. The study also reveals that:

- The fluid velocity accelerates with enhancement in the heat source term Q and Grashof number Gr magnitude. However, augmenting the Darcy term Da, suction S term, velocity slip α, stretching term λ, Hartmann number M,

power-law exponent m as well as Weissenberg value We decelerates the velocity profiles.

- A damped in the thermal boundary structure and the corresponding surface temperature distribution falls with a rise in the mass suction term S, Prandtl number Pr and thermal slip term b.

- A rising thermal boundary film viscosity structure is formed with increasing the fluid heat conduction term ζ, radiative heat term Nr, Darcy number as well as the heat source parameter Q.

References

[1] T. Abbas, S. Rehman, A. S. Muhammad & I. Utmankhel, "Analysis of MHD Carreau fluid flow over a stretching permeable sheet with variable viscosity and thermal conductivity", Physica A: Statistical Mechanics Applications **551** (2020) 215.

[2] S. O. Salawu, A. M. Obalalu & MD. Shamshuddin, "Nonlinear solar thermal radiation efficiency and energy optimization for magnetized hybrid Prandtl-Eyring nanoliquid in aircraft", Arabian Journal for Science and engineering **22** (2022) 070801.

[3] S. Sarkar, & O. D. Makinde, "Slip and temperature jump effects of MHD stagnation point flow towards a translating plate considering nonlinear radiations", Heat Transfer (2022). https://doi.org/10.1002/htj.22664.

[4] S. Nadeem, R. Mehmood & N. S. Akbar, "Combined effects of magnetic field and partial slip on obliquely striking rheological fluid over a stretching surface", Journal of magnetism and Magnetic Materials **378** (2015) 457.

[5] B. C. Sakiadis, "Boundary-layer behavior on continuous solid surfaces: I. Boundary-layer equations for two-dimensional and axisymmetric flow", AIChEJ **7** (1961) 26.

[6] L. J. Crane, "Flow past a stretching plane", Angew. Math. Phys. **21** (1970) 645.

[7] C. Y. Wang, "Flow due to a stretching boundary with partial slip an exact solution of the Navier-Stokes equations", Chem. Eng. Sci. **57** (2002) 3745.

[8] K. S. Tshivhi, O. D. Makinde & R. L. MonaledI "Unsteady MHD nanofluid convection with heat transfer over a stretching and vertically moving sheet", Proceedings of The Romanian Academy, Series A **23** (2022) 267.

[9] A. M. Okedoye, S. O. Salawu & E. A. Asibor, "A convective MHD double diffusive flow of a binary mixture through an isothermal and porous moving plate with activation energy", Computational Thermal Sciences: An Int. J. **13** (2021) 45.

[10] K. Zaimi & A. Ishak, "Stagnation-point flow towards a stretching vertical sheet with slip effects", MDPI Mathematics **4** (2016) 27.

[11] S. O. Salawu, R. A. Kareem & J. O. Ajilore, "Eyring-Powell MHD nanoliquid and entropy generation in a porous device with thermal radiation and convective cooling", Journal of the Nigeria Society of Physical Sciences **11** (2022) 833.

[12] H. Upreti, A. K. Pandey, M. Kumar & O. D. Makinde, "Ohmic heating and non-uniform heat source/sink roles on 3d darcy–forchheimer flow of CNTs nanofluids over a stretching Surface", Arab J Sci Eng. **45** (2020) 7705.

[13] P. Sreenivasulu, T. Poornima & N. B. Reddy, "Influence of Joule Heating and Non-Linear Radiation on MHD 3D Dissipating Flow of Casson Nanofluid past a Non-Linear Stretching Sheet", Nonlinear Engineering **8** (2019) 661.

[14] E. O. Fatunmbi & S. S. Okoya, "Heat transfer in boundary Layer magneto-micropolar fluids with temperature-dependent material properties over a stretching sheet", Advances in Materials Science and Engineering (2020) 1.

[15] S. O. Salawu, A. D. Ohaegbue, R. A. Kareem & A. R. Hassan, "On the hydromagnetic reaction of Oldroyd 8-constant Arrhenius exothermic fluid and explosion slice-chain in a plane Couette", Chemical Physics Impact **4** (2022) 100067.

[16] S. O. Salawu, E. O. Fatunmbi & S. S. Okoya, "MHD heat and mass transport of Maxwell Arrhenius kinetic nanofluid flow over stretching surface with nonlinear variable properties", Results in Chemistry **3** (2021) 100125.

[17] A. R. Hassan, S. O. Salawu, A. B. Disu & O. R. Aderele, "Thermodynamic analysis of a tangent hyperbolic hydromagnetic heat generating fluid in quadratic Boussinesq approximation", Journal of Computational Mathematics and Data Science **4** (2022) 100058.

[18] A. M. Alsharif, A. I. Abdellateef & Y. A. Elmaboud, "Electroosmostic flow of fraction Oldroyd-B fluid through a vertical microchannel filled with a homogenous porous medium: Numerical and semi-analytical solutions", Heat Transfer (2022). https://doi.org/10.1002/htj.22488.

[19] S. U. Mamatha, C. S. Raju, K. Mahesha & O. D. Makinde, "Radiative and viscous ohmic dissipation on MHD tangent hyperbolic fluid over a convectively heated sheet in a suspension of dust particles", Diffusion Foundations **16** (2018) 177.

[20] M. I. Khan, A. Tufail, T. A. Khan, S. Qayyum, T. Hayat, M. M. Khan & A. Alsaedi, "Entropy generation optimization and activation energy in nonlinear mixed convection flow of a tangent hyperbolic nanofluid", Eur. Phys. J. Plus **133** (2019) 1.

[21] B. Mahanthesh & J. Mackolil, "Flow of nanoliquid past a vertical plate with novel quadratic thermal radiation and quadratic Boussinesq approximation: sensitivity analysis", Int Commun Heat Mass Transfer **120** (2021) 105040.

[22] I. S. Oyelakin & P. Sibanda, "Analysis of exponentially varying viscosity and thermal conductivity on a tangent hyperbolic fluid", SeMA **77** (2020) 257.

[23] L. Sophus & M. Ackerman, "Sophus Lies 1884 Differential Invariant Paper", Math Sci. Press (1976).

[24] S. O. Salawu & M. S. Dada, "Lie group analysis of soret and dufour effects on radiative inclined magnetic pressure-driven flow past a Darcy-forchheimer medium", J. of the Serbian SoC. for computational Mechanics **12** (2018) 108.

[25] U. Zakir & G. Zaman, "Lie group analysis of magnetohydrodynamic tangent hyperbolic fluid flow towards a stretching sheet with slip conditions", Heliyon **3** (2017) e00443.

[26] Z. Ullah & G. Zaman, "Lie group analysis of magnetohydrodynamic tangent hyperbolic fluid flow towards a stretching sheet with slip conditions", Heliyon **3** (2017) e00443.

[27] Z. Ullaha, G. Zamana & A. Ishak, "Magnetohydrodynamic tangent hyperbolic fluid flow past a stretching sheet", Chinese Journal of Physics **66** (2020) 258.

[28] F. Shahzad, W. Jamshed, T. Sajid, MD. Shamshuddin, R. Safdar, S. O. Salawu, M. R. Eid, M. B. Hafeez & M. Krawczuk, "Electromagnetic control and dynamics of generalized Burgers nanoliquid flow containing motile microorganisms with Cattaneo-Christov relations: Galerkin finite element mechanism", Applied Sciences **12** (2022) 8636.

[29] A. M. Alsherif, A. I. Abduellateef, Y. A. Elmaboud & S. I. Abdesalam, "Performance enhancement of a DC-operated micropump with electroosmosis in a hybrid nanofluid: Fractional Cattaneo heat flux problem", Applied Maths. and Mechanics **43** (2022) 931.

[30] T. Hayat, I. Ullah, K. Muhammad & A. Alsaedi, "Gyrotactic microorganism and bio-convection during flow of Prandtl-Eyring nanomaterial", Nonlinear, Engineering **10** (2021) 201.

[31] I. Ullah, M. Alghamdi, W. F. Xia, S. I. Shah & H. Khan, "Activation energy effect on the magnetized-nanofluid flow in a rotating system considering the exponential heat source", Int. Commun. Heat Mass Transf. **128** (2020) 105578.

[32] Z. Aziz, & M. Shams, "Entropy generation in MHD Maxwell nanofluid flow with variable thermal conductivity, thermal radiation, slip conditions, and heat source", AIP Advances **10** (2020) 015038.

[33] C. Sumalatha & S. Bandari, "Effects of Radiations and Heat Source/Sink on a Casson Fluid Flow over Nonlinear Stretching Sheet", World Journal of Mechanics **5** (2015) 257.

[34] I. L. Animasaun, "Effects of thermophoresis, variable viscosity and thermal conductivity on free convective heat and mass transfer of non-Darcian MHD dissipative Casson fluid flow with suction and nth order of chemical reaction", J. of Nigeria Mathematical Society (2014) 1.

[35] S. O. Salawu, A. M. Obalalu, E. O. Fatunmbi & R. A. Oderinu, "Thermal Prandtl-Eyring hybridized MoS2-SiO2/C3H8O2 and SiO2-C3H8O2 nanofluids for effective solar energy absorber and entropy optimization:

A solar water pump implementation", Journal of Molecular Liquids **361** (2022) 119608.

[36] N. S. Akbar, S. Nadeem, R. U. Haq & Z. H. Khan, "Numerical solutions of Magnetohydrodynamic boundary layer flow of tangent hyperbolic fluid towards a stretching sheet. Indian Journal of Physics **87** (2013) 1.

[37] M. Fathizadeh, M. Madani, Y. Khan, N. Faraz & S. Tutkun, "An effective modification of the homotopy perturbation method for MHD viscous flow over a stretching sheet", J. King. Saud. University Sci. **25** (2013) 107.